Optics Communications 285 (2012) 5229–5234

Contents lists available at SciVerse ScienceDirect

Optics Communications

journal homepage: www.elsevier.com/locate/optcom

Omnidirectional antireflective properties of porous tungsten oxide films with in-depth variation of void fraction and stoichiometry

Nikolaos Vourdas [a], Konstantinos Dalamagkidis [b], Ioannis Kostis [a], Maria Vasilopoulou [a,]*, Dimitrios Davazoglou [a]

[a] NCSR Demokritos, Institute of Microelectronics, Terma Patriarchou Gregoriou, 15310 Athens, Greece
[b] Institut für Informatik VI, Technische Universität München (TUM), Boltzmannstraße 3, 85748 Garching bei München, Germany

ARTICLE INFO

Article history:
Received 21 June 2012
Received in revised form
26 July 2012
Accepted 1 August 2012
Available online 25 August 2012

Keywords:
Tungsten oxide
Hot wire deposition
RCWA
Antireflective coatings

ABSTRACT

We report on the fabrication of porous hot-wire deposited WO_x ($hwWO_x$) films with omnidirectional antireflective properties coming from in-depth variation of both (i) void fraction from 0% at the Si substrate/$hwWO_x$ interface to 30% within less than 7 nm and to higher than 50% at the $hwWO_x$/air interface, and (ii) x, namely $hwWO_x$ stoichiometry, from 2.5 at the Si/$hwWO_x$ to 3 within less than 7 nm. $hwWO_x$ films were deposited by means of hw deposition at rough vacuum and controlled chamber environment. The films were analyzed by Spectroscopic Ellipsometry to extract the graded refractive index profile, which was then used in a rigorous coupled wave analysis (RCWA) model to simulate the antireflective properties. RCWA followed reasonably the experimental reflection measurements. Void fraction and x in-depth variation, controlled by the hw process, greatly affect the antireflective properties, and improve the omnidirectional and broadband characteristics. The reflection suppression below 10% within the range of 500–1000 nm for angles of incidence up to more than 60° is demonstrated.

© 2012 Elsevier B.V. All rights reserved.

1. Introduction

In the last years the research activity in the area of solar cells has increased and has brought many solutions in order to achieve optimized efficiencies. To approach an optimal performance and to maximize efficiency broadband, antireflective coatings (ARC) are necessary [1].

The standard double layer antireflection coatings typically have a bandwidth lower than one octave, e.g., 400–700 nm [2], while solar cells require an antireflection coating operating in a broader range (e.g., 400–1700 nm) [3]. Thin films exhibiting thickness-graded refractive index profiles are being intensively studied recently, for applications in antireflective coatings with enhanced omnidirectionality and broadband characteristics [4]. The refractive index profile and hence the reflection suppression, is controlled either by depositing layers of different materials or by controlling the in-depth void fraction variation using multiple deposition steps, by employing various types of lithography and subsequent pattern transfer such as plasma etching, by incorporating particles and properly tuned deposition processes etc [5–11]. Even though most of these coatings exhibit good AR performance, the scale-up and the integration of most of these processes are either difficult or subject to serious economic constraints.

Recently we reported a simple method for depositing metal oxide films with their stoichiometry depending on the composition of the deposition ambient. It was found before that highly porous, stoichiometric ($hwWO_3$) films were deposited at 0.1 Torr of N_2. Due to their high porosity these films exhibited refractive index depending on thickness (i.e., deposition time) varying between 2 for thinner films and 1.2 for thicker ones, within the visible range [12]. By switching the deposition ambient from N_2 to H_2, sub-stoichiometric films, described as $hwWO_x$ with $x<3$, were also obtained, with their degree of stoichiometry (x) and refractive index depending on the exact H_2 partial pressure [13–15].

The aim of this work is to synthesize thin $hwWO_x$ films with improved omnidirectional AR performance, using hot-wire deposition, which is an easily implemented method as described before. In particular, here we present for the first time the fabrication of porous tungsten oxide films with graded refractive index, by varying the deposition ambient which initially contains H_2 and then switched to N_2 and we study their reflection performance. It is also shown that these films exhibit controllable in-depth profile of refractive index stemming from both the

* Corresponding authors.
E-mail addresses: nvourdas@imel.demokritos.gr (N. Vourdas), mariva@imel.demokritos.gr (M. Vasilopoulou).

0030-4018/$ - see front matter © 2012 Elsevier B.V. All rights reserved.
http://dx.doi.org/10.1016/j.optcom.2012.08.020

variation of stoichiometry and that of void fraction. The antireflective performance of thin and ultra-thin hwWO_x films on Si and the significant reflection suppression, below 10%, within the broad range of 500–1000 nm, is presented.

2. Experimental

2.1. Tungsten oxide films fabrication

Depositions of hwWO_x films were carried out in a hot-wire deposition system by heating the W filament in an ambient containing N_2 and H_2. The system was containing a stainless steel vacuum chamber (reactor) in which the substrate was positioned on a copper susceptor 5 cm below the heated W filament. An AC (50 Hz) current was used to heat the filament, and the temperature was monitored in situ, in order to calibrate electric current vs. filament temperature variation. Gases were injected into the reactor by a showerhead placed above the substrate; the corresponding flows were controlled by a gas line containing mass flow controllers (MFCs), valves and tubing. The pressure was monitored by a capacitance manometer (baratron), whose signal was used as input to a PC and the last was automatically driving a throttling valve placed between the chamber and the pumping system. The tungsten filament was heated at temperatures of 920 K, 1020 K and 1070 K. These temperatures are relatively low, compared to works from other groups, thus allowing only the surface oxide layer to be evaporated and not the metallic W. This feature provides additional advantages that are presented and discussed elsewhere [16]. Si pieces with dimensions of 2×2 cm^2 cut from (1 0 0) Si wafers were used as substrates. Before deposition the substrates were given a piranha clean, washed in ultra-pure water, dried in a nitrogen stream and loaded into the chamber. After loading, the chamber was evacuated below 1.33 Pa and then the pressure was stabilized to 133.3 Pa with the aid of a flow of H_2 or N_2 while keeping the throttling valve fully open. After pressure stabilization the filament was turn on. Deposition time was used to control film thickness and the times used varied between 1 s and 60 s. Due to the short deposition times and the high thermal mass of the copper susceptor, the substrate temperature was remaining near room temperature during deposition. After turning-off the filament, samples were left to cool down to room temperature while the pressure and the ambient used for the deposition were maintained. The cooling down was enduring several minutes.

2.2. Film optical and morphological characterization

Deposited hwWO_x films were characterized with a variety of techniques including spectroscopic ellipsometry (SE) within the 350–1000 nm range using a J.A Woolam Inc. M2000F rotating compensator ellipsometer (RCE^{TM}) running the WVASE32 software at an angle of incidence (AOI) of 75.14°.

The unmonochromatized Mg K_a line at 1253.6 eV (15 keV with 20 mA anode current) and an analyzer (Leybold EA-11) pass energy of 100 eV, giving a full width at half maximum, FWHM, of 1.3 eV for the Au 4f $_{7/2}$ peak, were used in all X-ray photoelectron (XPS) spectra measurements. The oxide stoichiometry was estimated using the XPS-measured W 4f and O 1s core-level spectra. To this extent, the areas under the photoemission peaks were integrated by fitting the O 1s and W 4f spectra with asymmetric Gaussian–Lorentzian curves.

A LEO Supra 35 VP scanning electron microscope (SEM) was used to characterize films morphology.

Specular optical reflectivity measurements were performed using the optical reflectometer FR-Basic by ThetaMetrisis S.A. (without integrating sphere) at near to normal AOI, using Tungsten white light source and spectrometer, and running the FR-Monitor software. An Al mirror with protective coating from Edmund Optics was used for reflection calibration.

3. Results and discussion

Tungsten oxide films were deposited with the hot-wire (hw) method using either N_2 or H_2 environment or a combination of both (switching the one after the other). Anticipating for

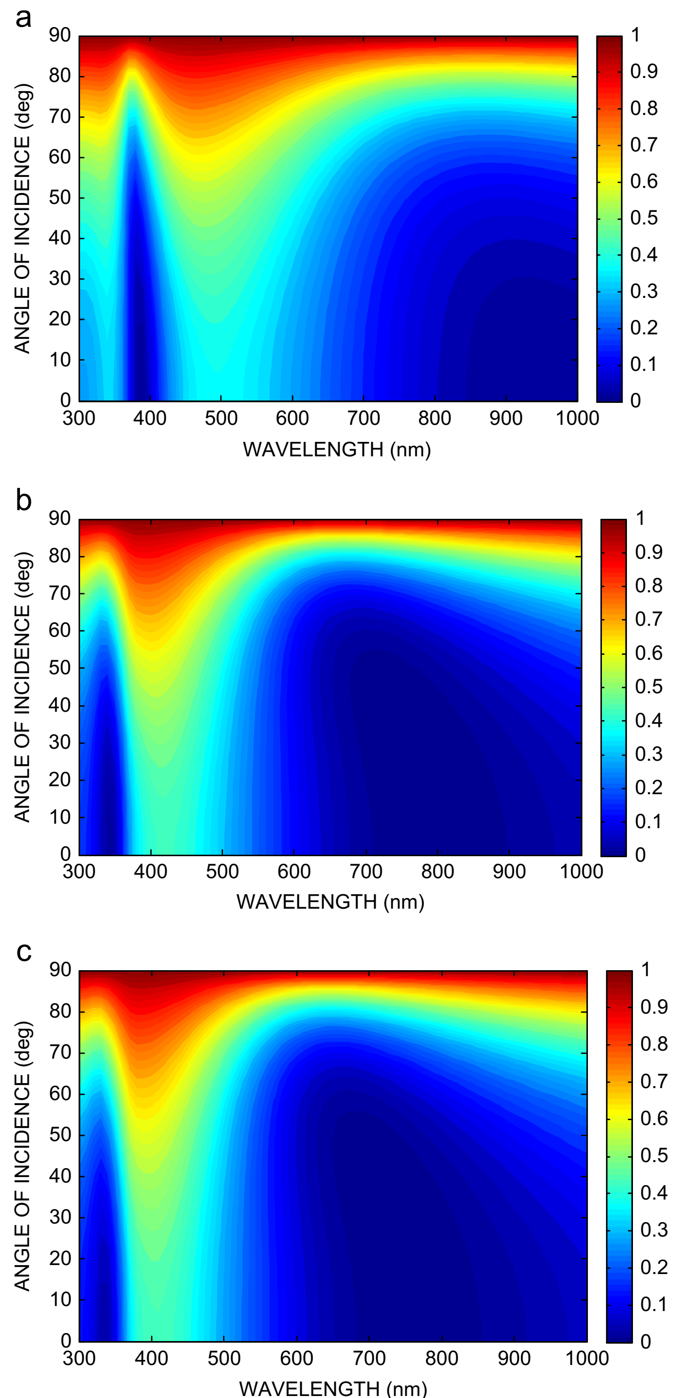

Fig. 1. Reflection calculated from RCWA for a hwWO_x/Si system with hwWO_x thickness in all cases equal to 107 nm. (a) Dense, non-porous stoichiometric hwWO_3, (b) 30% porous stoichiometric hwWO_3 and (c) 30% porous stoichiometric hwWO_x with graded refractive index profile as presented in Fig. 5(a). The total area on the figures for which reflection is below 10% increases from approximately 17% in (a) to 35% in (b) and to 37% in (c).

modeling details presented next, the calculated reflection of a Si substrate covered with a 107 nm thick layer of $hwWO_x$ and for Angles of Incidence (AOI) varying between 0 and 90° is shown in Fig. 1. Calculations were based on the rigorous coupled wave analysis (RCWA), and we focus in the region of 500–1000 nm which is of great importance, for example, for Si solar cells. Results in Fig. 1(a) pertain to a homogeneous, stoichiometric and compact layer of $hwWO_3$ on Si and demonstrates that reflection values below 10% exhibit only for wavelengths above 800 nm and AOIs of up to 30° for approximately a region of 17% of the total area in Fig. 1(a). This low reflection (reflection $<10\%$) area increases to 35% for a porous $hwWO_3$ film exhibiting 30% porosity as seen in Fig. 1(b). Finally, a graded refractive index profile (see Fig. 5(a) for the detailed profile), causes a further increase of this area to 37% by improving the omnidirectionality by 3–4° and shifting the low reflection region towards lower wavelengths. In the case of inverse pyramid-like textured Si substrate, routinely used in Si solar cells manufacturing, an ARC coating such as the one described above will cause further decrease of the reflection seen in Fig. 1(b) and (c), as, e.g., shown for the case of TiO_2 ARC [11]. For cells operating under sun-tracking this will decrease the requirements of the tracker for precision and therefore its price, which is related to the total price of the electricity produced.

In order to tune the refractive index profile, depositions of $hwWO_x$ films were carried out in an ambient initially containing H_2 and then switched to N_2, in order to controllably change films stoichiometry. Also, different deposition times were used. X-ray photoelectron spectroscopy (XPS) has been applied to follow films stoichiometry. The evolution of the oxide reduction was monitored by measuring the intensity of the W 4f core levels and calculating the ratio between the W^{6+} component versus the W components with lower oxidation states (e.g., 5+, 4+). By depositing the first layers of the film (e.g., the first 7 nm) under H_2 environment it was found that they were sub-stoichiometric WO_x (i.e., metallic [14]) with $x=2.5$ and their refractive index equal to 3. Then the deposition ambient was switched to N_2 resulting in the deposition of a ca. 100 nm gradually porous $hwWO_3$ layer. In Fig. 2(a) and (b) the XPS W 4f core levels of $hwWO_x$ layers deposited under N_2 and H_2 environment, respectively, are presented. The raw data after a Shirley background subtraction were fitted by a non linear least square routine using peaks with a mix of Gaussian and Lorentzian shape. In Fig. 2(a) the decomposition of W4f photoemission peak was performed using two equal width peaks (1 and 2) with binding energy of $W4f_{7/2}$ centered at 36.0 ± 0.1 eV. The spin orbit splitting of the doublet is 2.13 eV (and a peak ratio of 4:3) and a third broad peak of $5p_{3/2}$ is located at approximately 42 eV. The position and shape of these peaks are representative of W atoms with an oxidation state 6+, as expected for WO_3 [17]. For the substoichiometric film, the W 4f peak (Fig. 2(b)) becomes broader indicating that new spectral features appear. A decomposition of this spectrum is shown in Fig. 2(b). A new doublet was added (4 and 5) with spin-orbit splitting and peak ratio fixed at 2.13 eV and 4:3, respectively, with all peak widths equal to the peak width of the W $4f_{7/2}$ in Fig. 2(a). The binding energy of W $4f_{7/2}$ of the new doublet is at 34.8 eV and is attributed to the presence of W^{5+} atoms in WO_{3-x} [18]. The relative atomic concentrations in the analyzed region were calculated by dividing the total peak area of W 4f and O 1s (not shown here).

The surface atomic composition of the fully oxidized film as derived from the XPS measurements is: W: 1, O: 3.1 (±0.1) and of the reduced film: W: 1, O: 2.5 (±0.1). It should be mentioned that similar results for the reduced films composition were taken when either H_2 or forming gas was flowing into the chamber during film deposition. These results show that a compound with composition described by the formula $WO_{2.5}$ is formed. In this way $hwWO_x$ films with thickness-graded refractive index profiles with various thicknesses were synthesized. In Fig. 3 the cross-section (left) and top-view (right) scanning electron microscopy (SEM) images of these films are shown.

Similarly, another sample with total thickness of 78 nm was deposited. In order to extract the refractive index profile multiple depositions were carried out at various film thicknesses. In this way, a resolution of 2 nm was obtained for the first and top ca. 10 nm and of 10 nm for the remaining layer in between the interfaces. The reflection properties of these films at various AOI were calculated by means of RCWA and compared to experimental optical reflection measurements made at near to vertical incidence only. The details on optical measurements are given below. The deposited $hwWO_x$ films were characterized optically by means of SE. The beam spot projected on the sample sizes 2 mm long and therefore is in no case comparable to the characteristic diameter of the nanosized surface characteristics of the $hwWO_x$. SE has been previously implemented to examine reflection properties at various interfaces such as Si/SiO_2 [19], indium–tin–oxide (ITO) [20] and SiN_x [21] ARCs.

As reported before, in order to extract the refractive index profile many samples with various thicknesses were deposited. So, after 1 s of deposition SE analysis yielded the refractive index of $hwWO_x$ ($x=2.5$). In order to analyze the sample deposited in 2 s we used a double layer model, with the lower layer consisting of $hwWO_{2.5}$. In order to investigate the presence of $hwWO_{2.5}$,

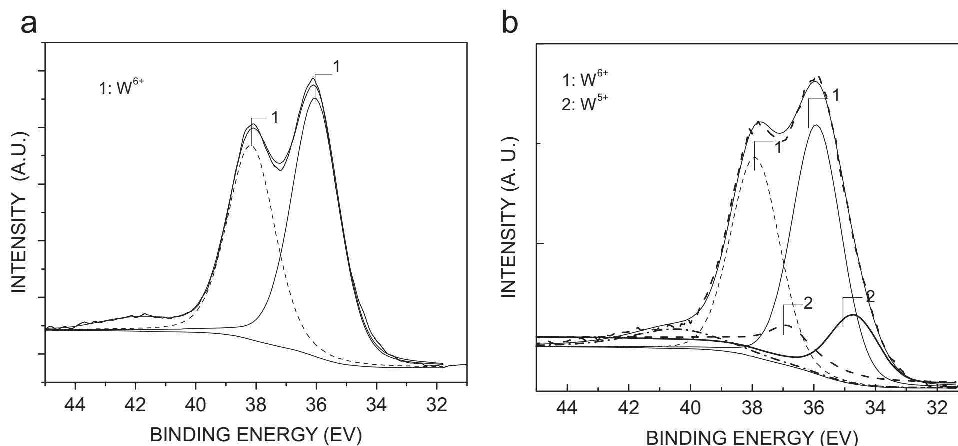

Fig. 2. X-ray photoelectron spectra of W 4f core levels of (a) stoichiometric $hwWO_3$ and (b) substoichiometric $hwWO_{2.5}$.

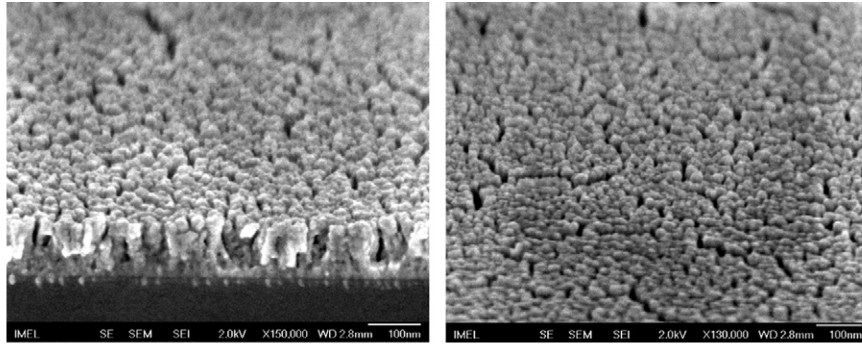

Fig. 3. SEM images of the 107 nm $hwWO_x$ stoichiometric film used for this study in (left) cross-section and (right) top-view.

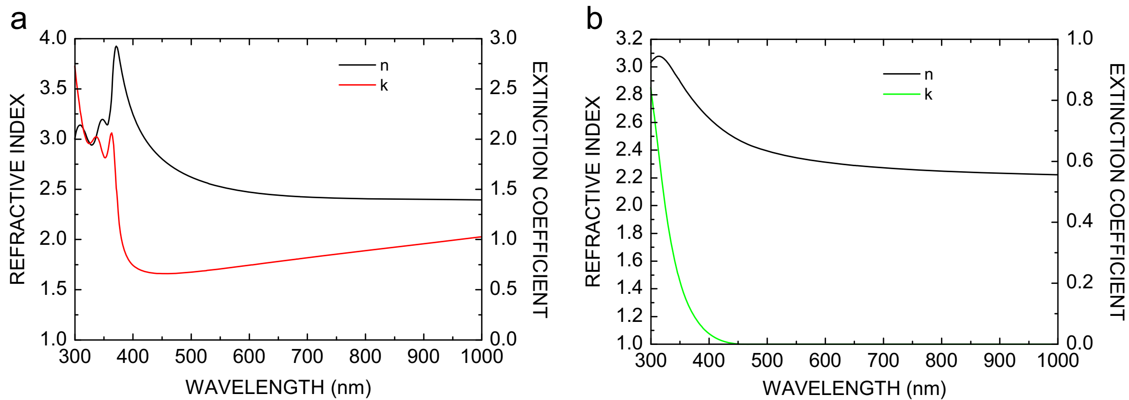

Fig. 4. Refractive index and extinction coefficient dispersion of (a) $hwWO_{2.5}$ (sub-stoichiometric) and (b) $hwWO_3$ (stoichiometric) used for this study.

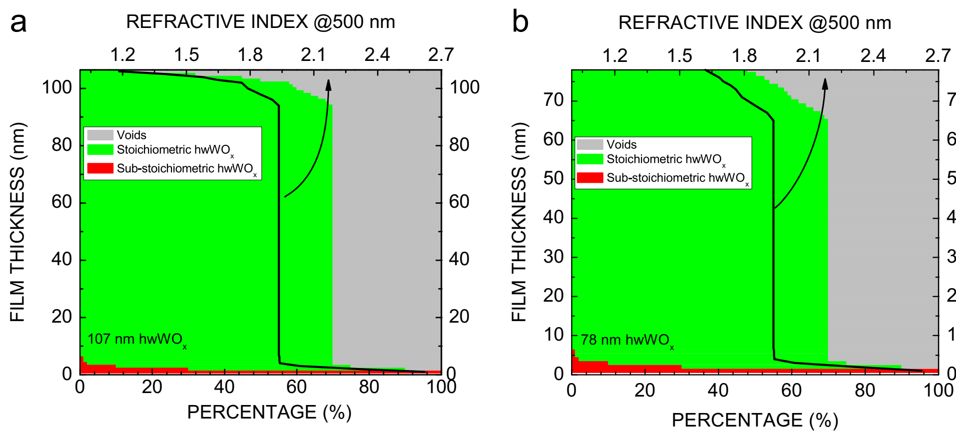

Fig. 5. Volume fraction of voids, of sub-stoichiometric and of stoichiometric $hwWO_x$ as modeled by means of SE for a (a) 107 nm and (b) 78 nm total thickness of $hwWO_x$. The respective in-depth variation of the effective refractive index (real part) @500 nm is also depicted.

$hwWO_3$, and voids in the upper layer, its optical properties were modeled with the aid of the Effective Medium Analysis (EMA) considering a mixture of the above and we extracted the corresponding volume fractions ($f_1(z)$, $f_2(z)$ and $f_3(z)$). The next sample was deposited at 5 s and was considered as a three-layer system the lower one consisting of $hwWO_{2.5}$, the intermediate one composed as described previously and the third one was again modeled using the EMA and the constituents considered for the intermediate layer and the volume fractions were extracted again. This procedure was followed for thicker films until reaching the final film thickness (78 nm and 107 nm).

The effective refractive index of each layer $\tilde{N}(z)=n-ik$, with $i=\sqrt{-1}$, is then approximated by the formula $\tilde{N}(z)=[f_1(z)\tilde{N}_1^q+f_2(z)\tilde{N}_2^q+(1-f_1(z)-f_2(z))\tilde{N}_3^q]^{1/q}$, with $q=2/3$ [22]. The optical properties of the sub-stoichiometric ($\tilde{N}_1$) and stoichiometric ($\tilde{N}_2$) $hwWO_x$ that used in this study are shown in Fig. 4(a) and (b) while for the voids $\tilde{N}_3=1$.

The $\tilde{N}(z)$ (only the real part) at 500 nm for a 107 nm and 78 nm thick $hwWO_x$ is shown in Fig. 5(a) and (b). Note that with this approach there is no need to assume a model for the geometry of the surface (composed of conical, pyramid, parabolic-like features) [23].

The fraction of the sub-stoichiometric $hwWO_{2.5}$, as seen in Fig. 5(a) and (b), starts from 100% and goes to zero within less than 7 nm, while at the same time the fraction of (stoichiometric) $hwWO_3$ gradually increases, along with the void fraction. This variation smoothes out the refractive index difference at the Si /$hwWO_x$ interface (at 500 nm Si: $n=4.29$, Substoichiometric $hwWO_x$: $n=2.63$, stoichiometric $hwWO_3$: $n=2.39$) and therefore suppresses the reflection at this interface. The formation

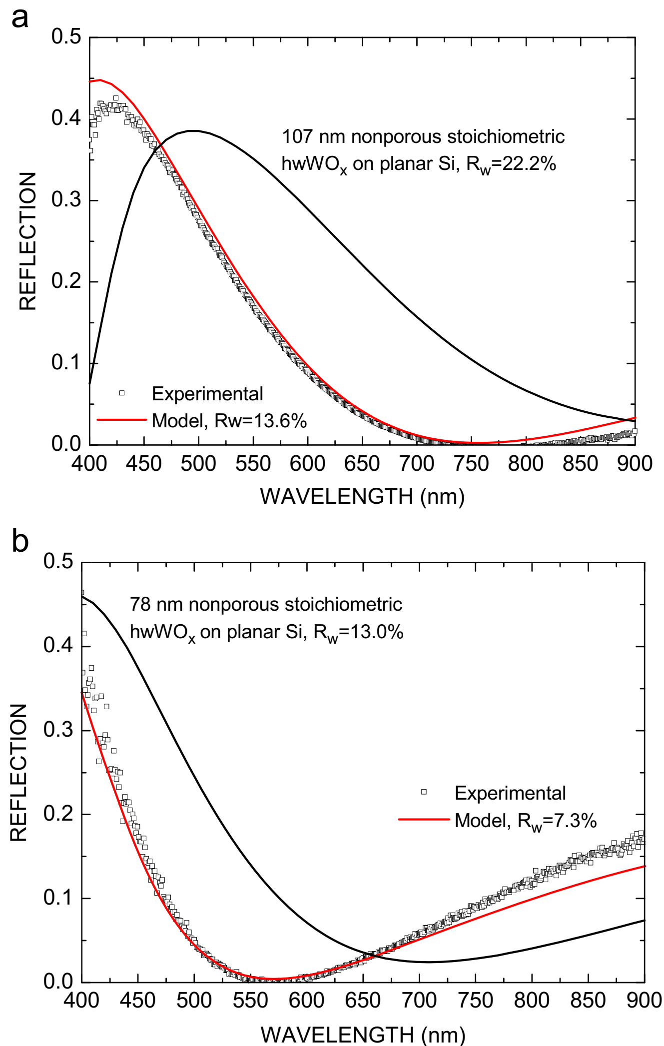

Fig. 6. Experimentally recorded and RCWA-calculated reflection for a (a) 107 nm and (b) 78 nm thick hwWO$_x$ film on Si wafer. Reflection for equally thick nonporous stoichiometric hwWO$_3$ films from RCWA are also illustrated for comparison purposes. Weighted average reflection for each case (R_w) is also depicted.

mechanism for this gradual decrease of sub-stoichiometric hwWO$_x$ fraction vs. film thickness, under reducing ambient is discussed elsewhere [13]. The void fraction of ~30% is kept essentially constant until the final ca. 10 nm, after which point the void fraction increases towards higher values (80% for the 107 nm film and 50% for the 78 nm film), resulting in a corresponding reduction of refractive index.

In Fig. 6 the experimentally measured reflection (with FR-Basic by ThetaMetrisis) for hwWO$_x$ films of thickness 107 nm and 78 nm is presented for wavelengths between 400 nm and 900 nm.

RCWA [24] was used to model reflection at vertical incidence (which corresponds to the first row of data at AOI=0 of Fig. 1 (c). In-depth variation in fraction of voids, hwWO$_3$ and hwWO$_{2.5}$ derived from SE, was used as input to RCWA (see Fig. 5(a) and (b)). Fig. 6 compares the RCWA results with experimental data showing a very good agreement, both in the absolute value of reflection and the position of minimum and maximum. For comparison purposes the calculated reflectance from equally thick nonporous stoichiometric hwWO$_3$ films on planar Si is also shown to show the clear deviation from our experimental data. In both cases the model of the non-porous stoichiometric hwWO$_x$ is shifted towards higher wavelengths as expected. The reflection suppression of our coatings compared to the equally thick nonporous films is also evidenced by the reduction of the weighted — to AM1.5 — average reflection (R_w), within the region 400–900 nm, which decreases from 22.2% to 13.6% and from 13.0% to 7.3% for the case of the 107 nm and 78 nm film, respectively.

4. Conclusion

Summarizing and concluding, it was shown that hot-wire metal oxide deposition is a simple method able to produce films exhibiting controllable in-depth profile of refractive index stemming from both the variation of stoichiometry and that of void fraction. The antireflective performance of thin and ultra-thin hwWO$_x$ films on Si was presented and a significant reflection suppression, below 10% within the range of 500–1000 nm, was shown for AOIs up to more than 60°. The deposition method allows for multiple switching of deposition ambient between N_2 and H_2 during the same run permitting further optimization of anti-reflection performance. SE analysis was employed to analyze the hwWO$_x$ optical properties layer by layer to extract the graded refractive index profile, which was subsequently used in the RCWA model to simulate the reflection properties. Our approach to simulate the reflection does not assume a specific model for the geometry of the surface, such as parabolic-, cone-like etc. The comparison between experimental and RCWA modeling results shows very good agreement. Film porosity along with the refractive index variations at the interfaces improves the omnidirectionality and broadband characteristics compared to the equally thick non-porous stoichiometric WO$_3$.

Acknowledgements

N. Vourdas was financially supported by the State Scholarships Foundation of Greece—Post Doctoral fellowship program. ThetaMetrisis S.A. is acknowledged for providing the optical reflection measurement setup (FR-Basic).

References

[1] W. Guter, J. Schöne, S.P. Philipps, M. Steiner, G. Siefer, A. Wekkeli, E. Welser, E. Oliva, A.W. Bett, F. Dimroth, Applied Physics Letters 94 (2009).
[2] D.S. Hobbs, B.D. MacLeod, J.R. Riccobono, Proceedings of SPIE-The International Society for Optical Engineering 2007.
[3] R.R. King, D.C. Law, K.M. Edmondson, C.M. Fetzer, G.S. Kinsey, H. Yoon, D.D. Krut, J.H. Ermer, R.A. Sherif, N.H. Karam, Advances in Opto Electronics (2007).
[4] J.Q. Xi, M.F. Schubert, J.K. Kim, E.F. Schubert, M. Chen, S.Y. Lin, W. Liu, J.A. Smart, Nature Photonics 1 (2007) 176.
[5] Y. Li, J. Zhang, S. Zhu, H. Dong, F. Jia, Z. Wang, Y. Tang, L. Zhang, S. Zhang, B. Yang, Langmuir 26 (2010) 9842.
[6] Y. Du, L.E. Luna, W.S. Tan, M.F. Rubner, R.E. Cohen, ACS Nano 4 (2010) 4308.
[7] S.A. Boden, D.M. Bagnall, Applied Physics Letters 93 (2008).
[8] S. Chhajed, M.F. Schubert, J.K. Kim, E.F. Schubert, Applied Physics Letters 93 (2008).
[9] N.E. Vourdas, M.E. Vlachopoulou, A. Tserepi, E. Gogolides, International Journal of Nanotechnology 6 (2009) 196.
[10] K. Choi, S.H. Park, Y.M. Song, Y.T. Lee, C.K. Hwangbo, H. Yang, H.S. Lee, Advanced Materials 22 (2010) 3713.
[11] B.S. Richards, Progress in Photovoltaics: Research and Applications 12 (2004) 253.
[12] G. Papadimitropoulos, N. Vourdas, K. Giannakopoulos, M. Vasilopoulou, D. Davazoglou, Journal of Applied Physics 109 (2011) 103527.
[13] M. Vasilopoulou, G. Papadimitropoulos, L.C. Palilis, D.G. Georgiadou, P. Argitis, S. Kennou, I. Kostis, N. Vourdas, N.A. Stathopoulos, D. Davazoglou, Organic Electronics 13 (2012) 796–806.
[14] M. Vasilopoulou, L.C. Palilis, D.G. Georgiadou, A.M. Douvas, P. Argitis, S. Kennou, L. Sygellou, G. Papadimitropoulos, I. Kostis, N.A. Stathopoulos, D. Davazoglou, Advanced Functional Materials 21 (2011) 1489.
[15] M. Vasilopoulou, L.C. Palilis, D.G. Georgiadou, P. Argitis, S. Kennou, L. Sygellou, I. Kostis, G. Papadimitropoulos, N. Konofaos, A.A. Iliadis, D. Davazoglou, Applied Physics Letters 98 (2011) 123301.

[16] N. Vourdas, G. Papadimitropoulos, I. Kostis, M. Vasilopoulou, D. Davazoglou, Thin Solid Films 520 (2012) 3614–3619.
[17] D. Barreca, S. Bozza, G. Carta, G. Rossetto, E. Tondello, P. Zanella, Surface Science (2003) 439–443, 532–535.
[18] M.J. Son, S. Kim, S. Kwon, J.W. Kim, Organic Electronics 10 (2009) 637.
[19] Y.J. Cho, Y.W. Lee, H.M. Cho, I.W. Lee, S.Y. Kim, Journal of Applied Physics 85 (1999) 1114.
[20] C.H. Chang, Y.P. Peichen, C.S. Yang, Applied Physics Letters 94 (2009).
[21] M.F. Saenger, J. Sun, M. Schädel, J. Hilfiker, M. Schubert, J.A. Woollam, Thin Solid Films 518 (2010) 1830.
[22] D.G. Stavenga, S. Foletti, G. Palasantzas, K. Arikawa, Proceedings of the Royal Society B: Biological Sciences 273 (2006) 661.
[23] K.C. Sahoo, Y. Li, E.Y. Chang, IEEE Transactions on Electron Devices 57 (2010) 2427.
[24] M.G. Moharam, E.B. Grann, D.A. Pommet, T.K. Gaylor, Journal of the Optical Society of America A: Optics and Image Science, and Vision 12 (1995) 1068.